Electrical Power and Energy Systems 62 (2014) 29–37

Contents lists available at ScienceDirect

Electrical Power and Energy Systems

journal homepage: www.elsevier.com/locate/ijepes

The direct-drive sensorless generation system for wave energy utilization

J.F. Pan [a], Yu Zou [a,b], Norbert Cheung [b], Guangzhong Cao [a,*]

[a] Shenzhen Key Laboratory of Electromagnetic Control, Shenzhen University, Shenzhen, Guangdong Province, PR China
[b] Department of Electrical Engineering, Hong Kong Polytechnic University, Hong Kong, China

ARTICLE INFO

Article history:
Received 1 July 2013
Received in revised form 8 April 2014
Accepted 9 April 2014
Available online 8 May 2014

Keywords:
Direct-drive
Sensorless
FEM
Linear switched reluctance generator

ABSTRACT

A direct-drive generator based on linear switched reluctance principle is investigated for wave energy utilization. Integrated with the sensorless technique, the direct-drive generator has the characteristics of low cost and robustness, and the power generation control system is especially suitable for the operation under hostile working environments since restrictions of physical sensors are eliminated. Simulation analysis based on the finite element methods (FEM) and joint simulation are carried out for performance analysis of the power generation control system, including position estimation, open loop turn-on and turn-off position optimization and closed loop current regulation. Experimental results validate the effectiveness of the position estimation scheme for the sensorless, linear switched reluctance generator based power generation control system.

Introduction

The earth is covered with 71% of ocean and it is estimated that an extractable power of more than 1 TW can be expected from wave energy globally [1]. Since wave energy originates from wind, wave motion exhibits low-speed translational characteristics, typically with the speed range of 0–2 m/s [2]. Nowadays, wave energy exploitation techniques mainly focus on indirect wave power conversion. By using mechanical linear-to-rotary translators such as the hydraulic or pneumatic converters, wave motion is transformed to high-speed rotary movement to propel high-speed generators for electricity [3–5]. Wave energy converters (WECs) that are considered to possess commercial values are the Pelamis from Ocean Power Delivery [3], the wave dragon from Wave Dragon APS [4], and the Archimedes Wave Swing from BV-AWS [5], respectively. However, the traditional methods of wave power extraction discussed above have the disadvantages of a complex and expensive power generation control system, and they are hard to maintain and have low overall transformation efficiency [6]. Therefore, the above WECs still have not been widely applied for mass production since electricity generated from such WECs is not cost effective.

Recently, the direct-drive methodology for wave energy exploitation has been proposed. By direct capture of translational wave energy in one dimension, the linear generators can be employed to eliminate intermediate mechanical translators or converters. Therefore, the direct-drive method brings a simpler power take-off system with higher power efficiency. Current research mainly focuses on the linear synchronous permanent magnet generators (LSPMG). Though the LSPMGs have relatively large force-to-volume ratio and high conversion rate and efficiency, the involvement of permanent magnets (PMs) can result in the complicated machine winding scheme [7,8] or sophisticated arrangement and assembly of PMs [9]. Therefore, the overall manufacture and assembly cost for the power generation control system is high. Furthermore, temperature variations and machine saturation due to PMs can lead to performance degradation or even malfunction of the generation system [10].

The linear WECs based on the direct-drive methodology usually rely on physical sensors that detect position/velocity information for correct phase excitation or proper output voltage and current control. The physical sensors such as the linear optical or magnetic encoders require certain working limitations, especially the temperature range. However, the WECs often work under the rough and unattended environment and there will be many uncertainties and disturbances exercised on the generation system. The variations of wave extraction conditions such as humidity, wave impact and particularly temperature variations, unavoidably affect the standard working operation of these sensors, and this ultimately influences the stability and output performance of the system. In addition, the position/velocity sensors are one of

* Corresponding author. Address: S816, Fundamental Laboratory Building Phase II, Southern Campus of Shenzhen University, Shenzhen 518060, PR China. Tel.: +86 755 26535382; fax: +86 755 2655 7471.
E-mail address: cao_guang_zhong@163.com (G. Cao).

http://dx.doi.org/10.1016/j.ijepes.2014.04.017
0142-0615/

the indispensible factors for the cost of the power generation control system [11].

To solve the above problems, this paper investigates a direct-drive, sensorless, linear power generation control system based on switched reluctance principle. The linear generator has the characteristics of a simple and robust machine structure and it is suitable for the operation under hostile environment. The total manufacture cost is low and the machine is very suitable for mass production, since the switched reluctance machine itself is only composed of laminating steel sheets and copper wires. Material-wise, the proposed linear switched reluctance generator (LSRG) does not contain any expensive PMs or complex windings.

The position/velocity sensors is another factor for the total cost of the LSRG based power generation control system [12]. Therefore, the total system cost can be further reduced if such sensors can be eliminated by the integration of proper sensorless methods. By employing the pulse injection position detection technique, the sensorless approach is integrated on the LSRG based generation system. Therefore, the total cost of the power generation control system can be kept relatively low compared to the system from a LSPMG counterpart.

The paper is organized as follows. The principle of the LSRG and the sensorless technology are discussed in Section 2. Section 3 first investigates the characteristics of the LSRG based on finite element methods (FEM). Then simulation analysis for the power control system, position optimization in open loop and closed loop current regulation are performed for the LSRG-based generation system. Section IV focuses on the experimental validation of the sensorless power generation control system. Section V provides the conclusion and discussion remark.

Principle of the LSRG and sensorless technique

The LSRG and its symbols can be found in Fig. 1. It mainly consists of a moving platform, stator and a pair of linear guides to facilitate the linear motion along x axis. The LSRG has three-phase windings and it corresponds to a typical "6/4" rotary SR machine. The movers and the stator are made from laminated silicon-steel plates. Major machine parameters are listed in Table 1.

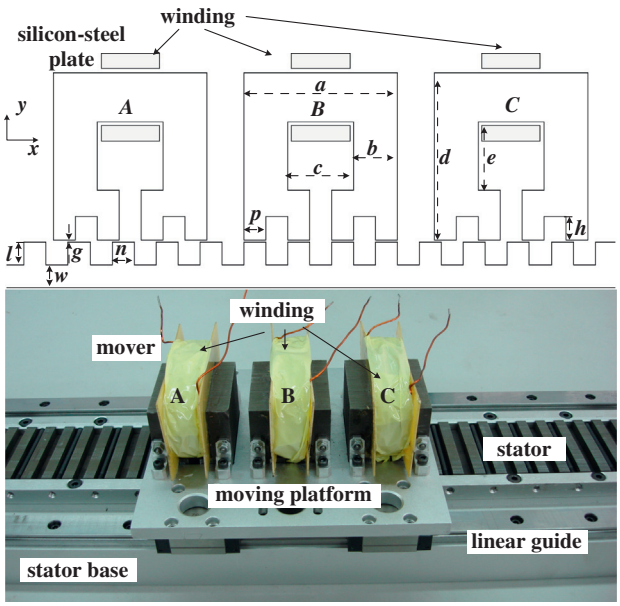

Fig. 1. The LSRG.

Table 1
Major machine parameters.

Parameter	Value	Parameter	Value
Mover pole width (a)	42 mm	Stator pole width (n)	6 mm
Mover yoke width (b)	12 mm	Stator pole height (l)	6 mm
Mover height (d)	44 mm	Stator yoke height (w)	6 mm
Height of winding slot (e)	18 mm	Air gap length (g)	0.5 mm
Width of winding slot (c)	18 mm	Stack length	50 mm
Mover pole height (h)	6 mm	Stroke length	450 mm
Mover pole width (p)	6 mm	Thickness of laminations	0.3 mm
Number of turns of each phase	160	Pole-pitch	12 mm

Theoretical background of the LSRG

The LSRG can be represented as a typical electromechanical system with one mechanical input and three electrical outputs. From the mechanical side,

$$F = M\frac{d^2s}{dt^2} + D\frac{ds}{dt} + f \tag{1}$$

where F stands for the mechanical force input, M is the mass of the moving platform, s is displacement, D is damping coefficient and f represents load force.

From the electrical terminal, the LSRG can be described in the form of voltage balance equation as [12],

$$u_j = R_j i_j + L_j\frac{d\lambda_j}{dt} \quad (j = A, B, C) \tag{2}$$

where u_j and λ_j represent voltage drop and flux-linkage of the j-th winding, respectively i and R are phase current and resistance. If the linear generator employs the typical three-phase asymmetrical

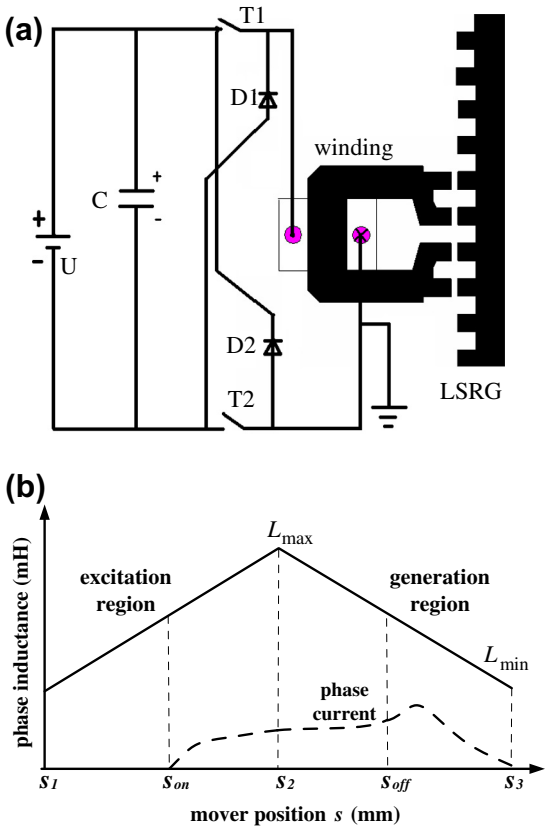

Fig. 2. (a) Drive topology of one phase and (b) turn-on and turn-off regulation.

half-bridge as drive topology as shown in Fig. 2(a), for any one phase, voltage can be expressed as,

$$\begin{cases} u_j - 2u_{Tj} = -e_j + R_j i_j & (T_1, T_2 - ON) \\ u_j - 2u_{Dj} = -e_j + R_j i_j & (D_1, D_2 - ON) \end{cases} \quad (3)$$

where u_T and u_D stand for the voltage drop of the power switch and the freewheeling diode and e is the generated electromotive force across the winding. If the LSRG operates in the linear region and mutual coupling effect can be neglected, for any phase, the change of excitation current during motoring can be represented as,

$$\frac{di_j}{ds} = \frac{u_j - 2u_{Tj}}{v_s \cdot L_j(s)} - \frac{\frac{\partial L_j(s)}{\partial s} \cdot v_s + R_j}{v_s \cdot L_j(s)} \cdot i_j(s) \quad (T_1, T_2 - ON) \quad (4)$$

If the diodes are turned on, the change of the generated current during generation process can be expressed as,

$$\frac{di_j}{ds} = \frac{u_j - 2u_D}{v_s \cdot L_j(s)} - \frac{\frac{\partial L_j(s)}{\partial s} \cdot v_s + R_j}{v_s \cdot L_j(s)} \cdot i_j(s) \quad (D_1, D_2 - ON) \quad (5)$$

with $j = A, B, C$, and v_s is velocity and L_j is the self inductance of the j-th phase.

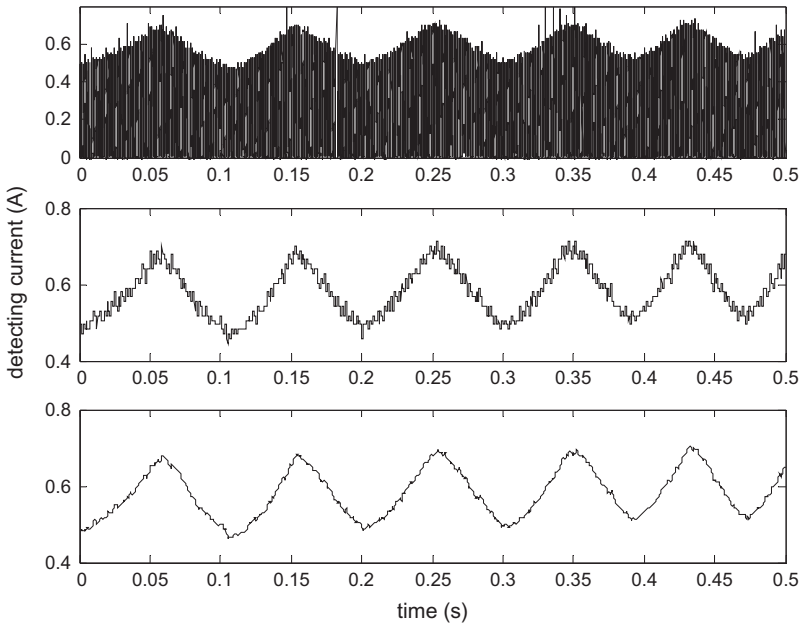

Fig. 3. Injected current pulse (upmost), sampling waveform before filtering (middle) and after filtering (lowest).

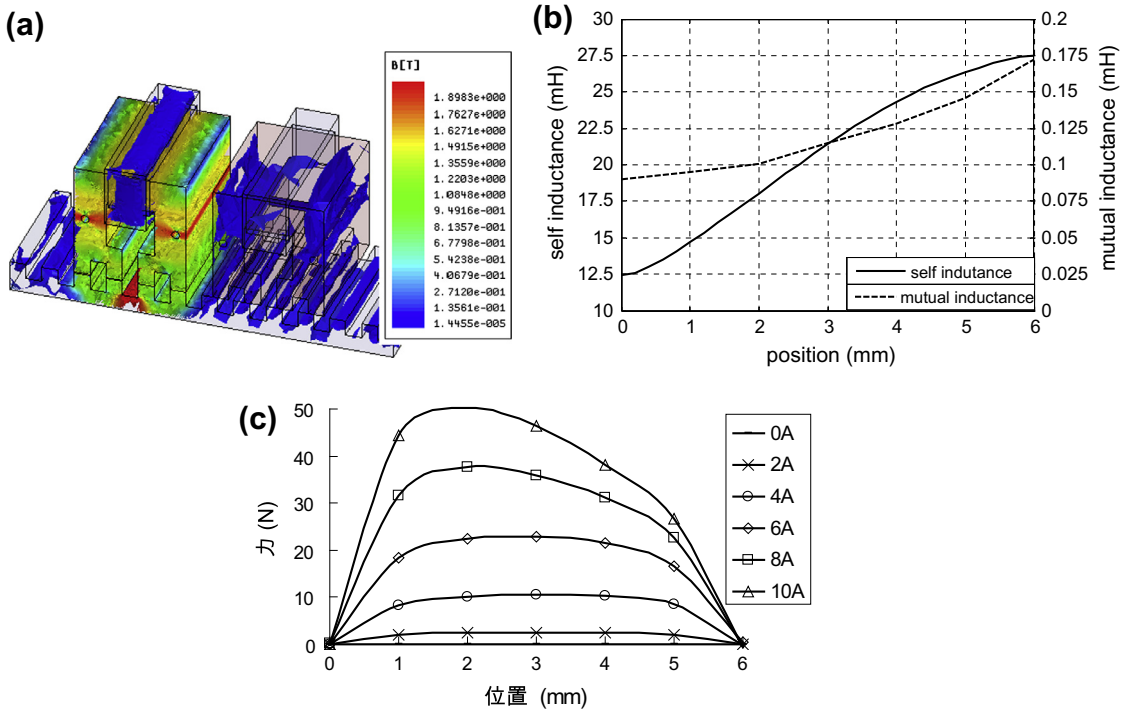

Fig. 4. Magnetic field distribution (a) mutual and self inductance (b) and (c) propulsion force.

Current regulation based on turn-on and turn-off positions

According to (4) and (5), current is the function with respect to displacement. Assuming that the linear inductance model is employed as shown in Fig. 2(b), for proper power generation of phase current output, the windings of the LSRG can be excited from a point s_{on} where the gradient of inductance is positive to a point s_{off} where the gradient of inductance is negative [12]. The phase

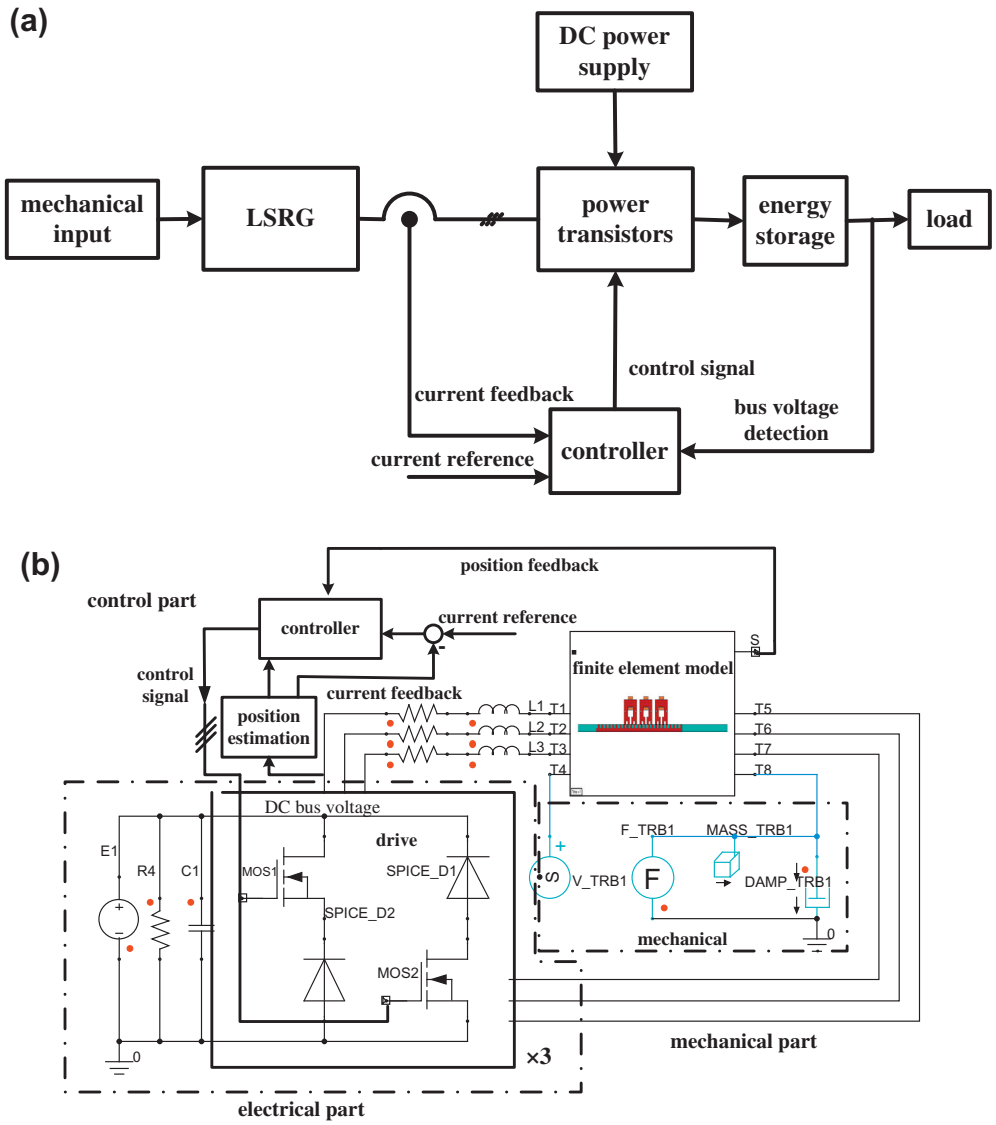

Fig. 5. Control diagram (a) and (b) control system schematic.

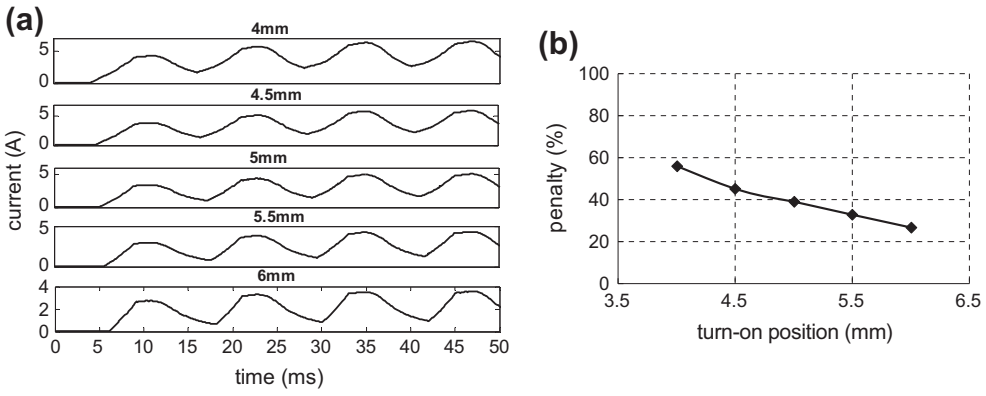

Fig. 6. Turn-on position regulation (a) phase current and (b) excitation penalty.

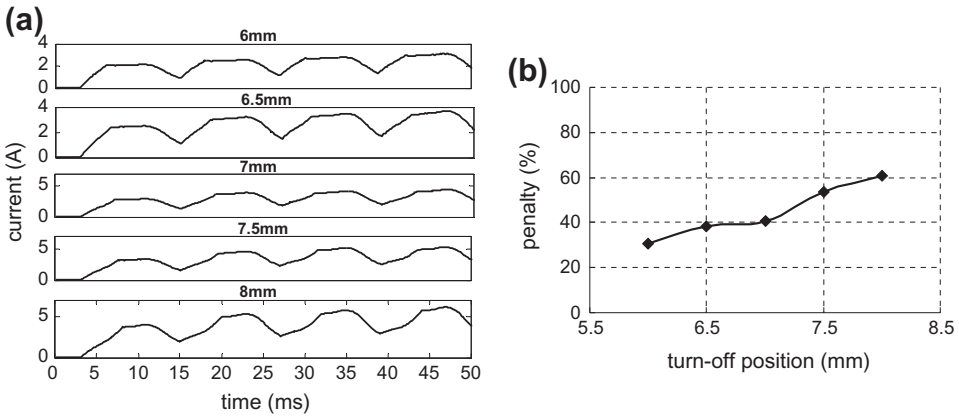

Fig. 7. Turn-off position regulation (a) phase current and (b) excitation penalty.

Table 2
Joint optimization of on and off positions.

	Turn-on position (mm)	Turn-off position (mm)	Value of excitation penalty (%)
a	2	5	40.6
b	3	6	32.7
c	4	7	29.6
d	5	8	27.3
e	6	9	27.0

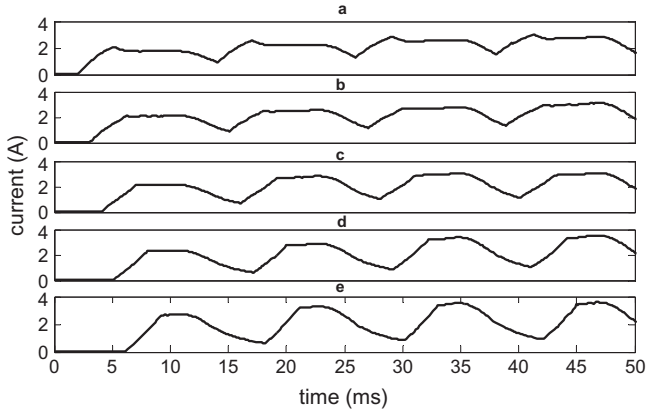

Fig. 8. Phase current output for joint optimization.

current of the LSRG can be derived from the following according to Fig. 2(b). The self inductance can thus be expressed as,

$$L(s) = \begin{cases} k_s(s_2 - s_1) + L_{\min}, & s_1 \leqslant s \leqslant s_2, \\ L_{\max} + k_s(s_3 - s_2), & s_2 \leqslant s \leqslant s_3. \end{cases} \tag{6}$$

If one of the three-phase movers of the LSRG translates from s_{on} to the fully aligned position s_2, substituting Eqs. (6) into (2) and neglecting phase resistance, the current of any one phase can be formulated as,

$$i_j(s) = \frac{u_j(s - s_{on})}{v_s \cdot [L_{\min} + k_s(s - s_1)]} \tag{7}$$

where k_s denotes the gradient of the inductance. If the mover continues to translate until the power switches are turned off at the position s_{off}, the phase current can be derived as,

$$i_j(s) = \frac{u_j(s - s_{on})}{v_s \cdot [L_{\min} + k_s(s - s_2)]} \tag{8}$$

If the mover translates from s_{off} to the next phase excitation period, the phase current can be represented as,

$$i_j(s) = \frac{u_j(s_{off} - s_{on} - s)}{v_s \cdot [L_{\max} + k_s(s - s_2)]} \tag{9}$$

Total power output P_o in one period of generation can be calculated by the following equation as,

$$P_o = \sum_{j=1}^{3} \frac{3}{T} \int_0^T u_j i_j dt \tag{10}$$

T is the period of the power generation control system. As discussed above, phase current is a function of s_{on} and s_{off} with a constant voltage drop u_j. The output power of the system can be further expressed as,

$$P_j = \frac{3 \cdot u_j^2}{v_s} f(s_{on}, s_{off}, L_j(s, i_j)) \tag{11}$$

It can be concluded from (11) that output power is proportional to the square of the bus voltage and inversely proportional to the speed of the generator if phase resistance can be neglected.

The efficiency of the generation system is formulated as,

$$\eta = \frac{P_o}{F \cdot v_s} \tag{12}$$

where η is the efficiency of power generation.

Table 3
Energized phase and detection phases.

Velocity (positive)	Detection phases	Energized phase	Velocity (negative)	Detection phases	Energized phase
0–3 mm	B,C	A	0–1 mm	C,A	B
3–7 mm	C,A	B	1–5 mm	A,B	C
7–11 mm	A,B	C	5–9 mm	B,C	A
11–12 mm	B,C	A	9–12 mm	C,A	B

Position estimation

Since the pulse injection method is suitable for position detection under the low speed operation, the impressed pulse current signal is employed for the LSRG without introduction of any extra hardware [13]. According to Eq. (2), neglecting mutual inductance, the voltage balance equation can be further expressed by,

$$U_i = R_j i_j + \frac{d\lambda(i_j, s)}{dt} = R_j i_j + \left(L_j + i_j \frac{\partial L_j}{\partial i_j}\right)\frac{di_j}{dt} + i_j \cdot v_s \cdot \frac{\partial L_j}{\partial s} \tag{13}$$

From Eq. (11), neglecting phase resistance, the output power is directly proportional to the square of the bus voltage and inversely proportional to the speed of the generator. However, since the excitation current value cannot reach infinity with limited voltage and phase resistance values, at zero speed, output power value cannot be infinitely great. This can be further verified by the last term of Eq. (13).

The value of the current can be obtained by solving the following equation [13],

$$i_j(t) = \frac{b_j}{a_j} \cdot U_j(1 - e^{-a_j t}), \quad j = A, B, C \tag{14}$$

where $a_j = \frac{R_j}{L_j}$, $b_j = \frac{1}{L_j}$.

According to Eq. (14), it can be concluded that mover's position can be derived from the maximum values of pulse currents [14,15]. The pattern of the injected current is shown in Fig. 3. The magnitude of the current is 0.7 A. A low pass filter with cut off frequency of 500 Hz is employed to regulate the phase current with no delay or oscillation in the position estimation process.

Excitation penalty

The excitation penalty ε for the LSRG can be defined as,

$$\varepsilon = \frac{I_{in}}{I_{out}} \times 100\% \tag{15}$$

where I_{in} is the average value of the energized current as the power transistors are turned on and I_{out} is the average value of the current between the time interval of power transistors switched off to the next power generation period. Under the same conditions, it is clear that the smaller the value of excitation penalty, the higher proportion of the transformed electric power to the total power. Therefore the excitation penalty can be employed to optimize the on–off position of the LSRG in open loop.

Wave energy basics

The energy of wave can be calculated based on the linear theory of small amplitude fluctuations including both kinetic and potential energy. Assuming that the height of the wave is ς, the wave surface can be expressed as [16],

$$\varsigma = A_1 \cdot \sin(k_1 \cdot x - \omega \cdot t) \tag{16}$$

where A_1 is the amplitude of wave, x is the displacement of wave with k_1 as the coefficient and ω is angular frequency. If the wave possesses a density of ρ, the kinetic energy of the wave within one wavelength can be expressed as,

$$E_k = \frac{1}{4}\rho g A_1^2 \varsigma \tag{17}$$

where g is acceleration of gravity. The total energy of the wave thus can be expressed as,

$$E = \frac{1}{2}\rho g A_1^2 \varsigma \tag{18}$$

According to total wave energy and the mechanical energy that the power generation control system absorbed, the proportion of the mechanical energy from the wave can be determined.

Simulation results

FEM simulation

To fully predict the generator performance, three-dimension (3D) finite element model is constructed in *MAXWELL* software. According to the machine structure, the magnetic circuit of the generator is short and the flux lines only circulate along the energized phase mover, the stator and the air gap between them. The 3D FEM model and magnetic field distribution of two adjacent phases can be found in Fig. 4(a). Fig. 4(b) shows self and mutual inductance values of the two phases from the fully aligned position (0 mm) to the fully un-aligned position. Though the mutual value at the fully un-aligned positions is the most significant, it is about 6.4% to the self inductance value at this position. Since each phase has the same dimensions and ratings, the mutual inductance values from any one phase to its closest one are considered the same and the coupling effect between phases can be neglected. The propulsion force of any one phase within half pole-pitch according to different current levels can be found in Fig. 4(c).

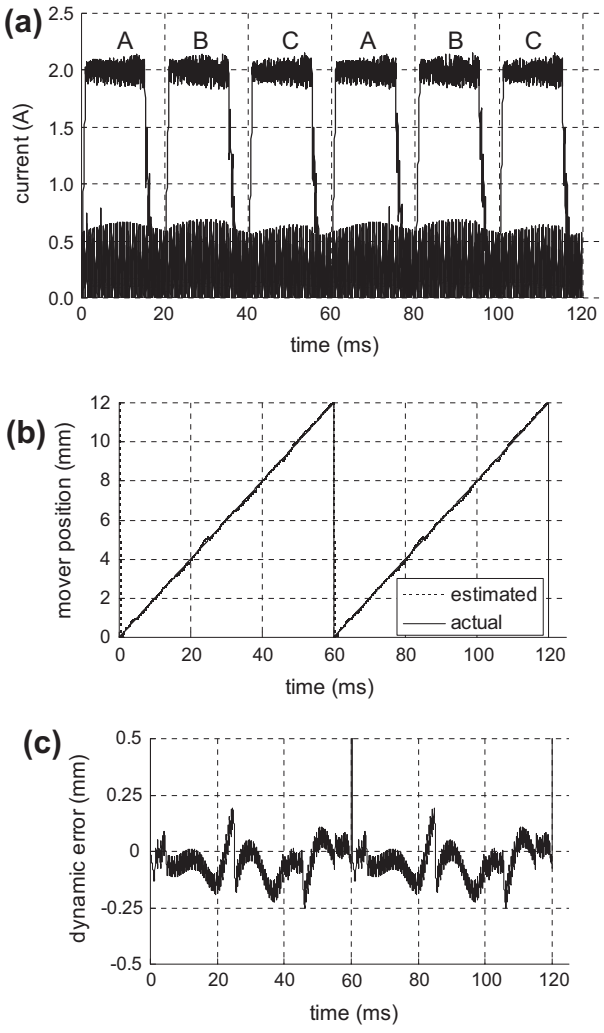

Fig. 9. Current output (a) estimated position (b) and dynamic error (c).

Joint simulation of the power control system

The entire power generation control system mainly consists of a direct current (DC) power source, the LSRG, a mechanical input to drive the LSRG, the power transistors, the controller, the capacitor and the load resistor, as shown in Fig. 5(a). Inspection of power generation is based on the multi-physics environment by co-simulation of *Maxwell* and *Simplorer* software package. The control system schematic can be found in Fig. 5(b). The finite element model of the LSRG designed in *Maxwell* is connected to the electrical part and the mechanical part, which are constructed in *Simplorer*. The electrical part includes the DC power resource, the power transistors, a capacitor and a load resistor. The mechanical part is composed of the mass of the mover and the damper, respectively. The position of the LSRG is estimated by monitoring the DC bus voltage and pulse phase current of the LSRG. The estimated position is supplied to the controller which controls the state of the power transistors.

Optimization of turn-on and turn-off position at nominal speed

Though the best performance in open loop of the LSRG depends on the power transistors at proper positions to switch on or off, for typical operation of power generation, nominal speed of 1 m/s is considered for turn-on and turn-off position optimization [17]. According to Fig. 2(b), the LSRG enters the generation region after the power transistors are switched off during the region of the declining inductance (6–12 mm). First, the turn-off position is fixed at 9 mm and the turn-on position is regulated to observe the phase current. For different turn-on positions from 4 to 6 mm, as shown in Fig. 6(a), it takes about 30–40 ms to settle with input speed of 1 m/s. The excitation penalty can be calculated according to (17) and the penalty profile can be found in Fig. 6(b).

The turn-off position can be optimized according to the value of excitation penalty as well. The turn-on position is fixed at 3 mm and the turn-off position is regulated from 6 to 8 mm. The phase current waveforms and the excitation penalty profiles are demonstrated in Fig. 7. The value of excitation penalty increases with turn-off positions and it can be obtained that 6 mm has the lowest percentage of excitation penalty. In order to obtain a lower excitation penalty and get a good performance of the generation system, the span from turn-on to turn-off should be limited at least 3 mm since it is beneficial to the power generation process [18].

After the interval from on to off is set as 3 mm for the generation system, joint optimization of turn-on and turn-off positions are conducted for the LSRG. The percentage values of excitation penalty are listed in Table 2 corresponding to phase current waveforms plotted in Fig. 8. From Table 2, the value of excitation penalty is decreased from state *a* to *e* and the overshoot of phase current in state *a* is the largest. For the condition of state *a* and *b*, since the direction of movement is the same to that of the propulsion force,

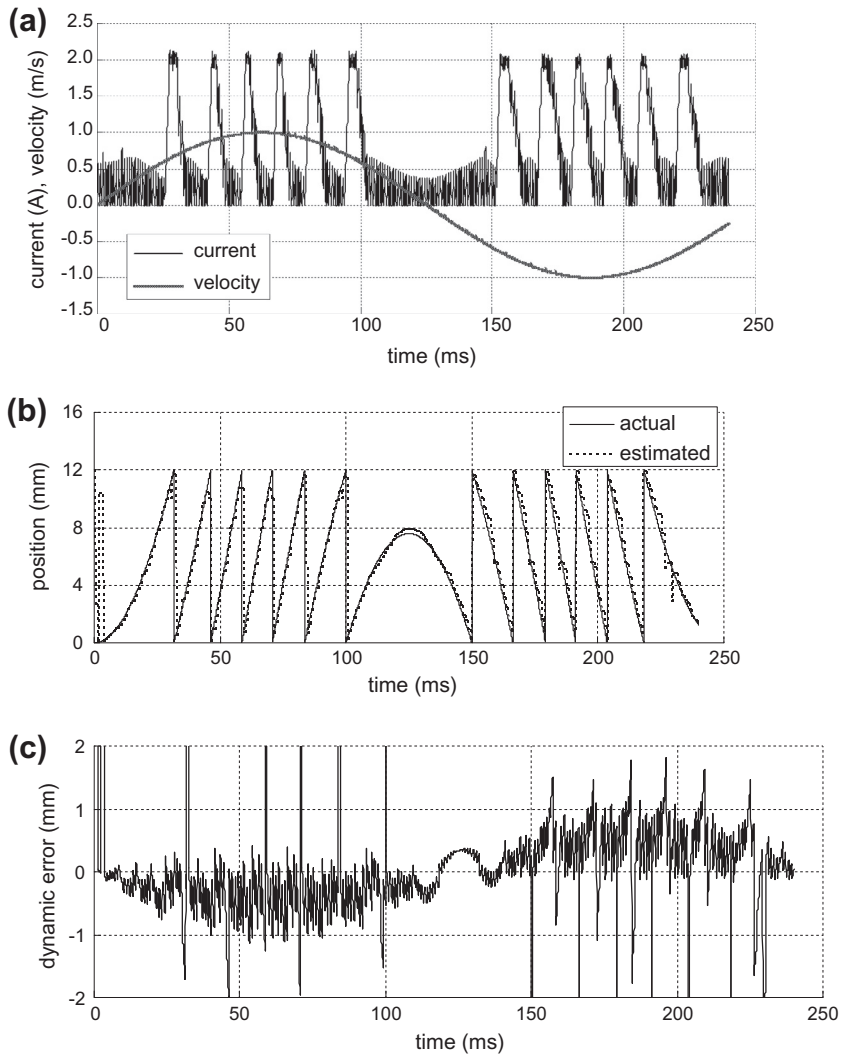

Fig. 10. Waveforms under sinusoidal speed (a) current of phase A, (b) estimated position and (c) dynamic error.

phase current output mainly derives from current freewheeling during the phase excitation period. In addition, the longer time the phase current can sustain the value of excited current, the better for the LSRG to translate mechanical energy [16]. Therefore, state *d* is selected as the optimized conducting position of the generation system considering both the phase current output and the value of excitation penalty.

Simulation of position estimation and power generation

The energized phase and detection phases corresponding to position of the mover is tabulated in Table 3. The original position (0 mm) of the LSRG is defined as the fully aligned position of phase A. As discussed above, the turn-on and turn-off positions for each phase mover are regulated according to 27.3% of excitation penalty. The simulation speed that propels the moving platform is first set as 0.2 m/s and the frequency of the detection pulse is 1 kHz, respectively. The maximum phase current output of the generation system is limited at 2 A by current chopping control for proper connection of energy storage components [16]. Current waveforms of the three phases can be found in Fig. 9(a). The estimated position and dynamic position error profiles are shown in Fig. 9(b) and (c), respectively. At the speed of 0.2 m/s, the absolute steady-state estimation error falls into 0.25 mm from the simulation results, except for the transitions from one pole-pitch to another where exist delays of position estimation.

To simulate dynamic wave motions, the input speed of the generation system is a sinusoidal waveform with amplitude of 1 m/s and frequency of 4 Hz, the current waveform of phase A can be found in Fig. 10(a). The estimated position and dynamic error profile are provided in Fig. 10(b) and (c), respectively. It can be concluded that dynamic error increases with the input speed. If the detection frequency is determined, the estimated position accuracy is inversely proportional to speed. Furthermore, time delay also increases with moving speed, limited by the calculation capability of the computation hardware [11].

Experimental validation

The experiment is carried out based on the control platform of dSPACE DS1104 board. The control program is developed under *MATLAB/SIMULINK* which can be downloaded to the digital signal processor of the controller board and control parameters can be modified online. Three commercial current amplifiers capable of inner current regulation are used to drive the double-sided linear switched reluctance motor (DLSRM) as the mechanical source of the LSRG-based power generation control system. The DLSRM and the LSRG are connected by a mechanical rod. The output parameters are regulated through the three-phase asymmetrical drive circuit and the energy storage components with the capacitor and the resistor in parallel. The currents signals are sampled by the three current sensors. The experimental set up is established as shown in Fig. 11(a).

As shown in Fig. 11(b), the phase current is regulated at 2 A under the frequency of detection pulse signal of 1 kHz and the speed input of 0.2 m/s. The estimated position and estimation error are given in Fig. 11(c) and (d), respectively. The asymmetry of the dynamic error profile results from the mechanical imperfections of the LSRG prototype. The delay that causes dynamic estimation error is worse compared to the simulation results. Another reason for large dynamic error is that the detecting pulse current signals are readily influenced by the noise populated from the working environment. Generally speaking, the dynamic errors fall into 1 mm, which proves that it is accurate enough for correct current excitation or generation.

The experimental results for variable speed with sinusoidal of maximum velocity of 1 m/s can be found in Fig. 12. Closed loop current regulation of 2 A is performed and results from Fig. 12(a) shows that the current peak values are larger compared to those from simulation. The same phenomena exist from Fig. 12(c), since the accuracy of current chopping is restricted by the hardware capability. There is a constant area from 120 to 140 ms for the position estimation profile as shown in Fig. 12(b). This is because the machine has mechanical inertia and it cannot reverse speed instantly. It can be concluded that the dynamic errors of estimation falls into 1.8 ms, and the experimental results correspond to the simulation ones, as shown in Fig. 12(c).

The power output is calculated according to (10) with results demonstrated in Fig. 12(d) from standstill to full speed. It is clear

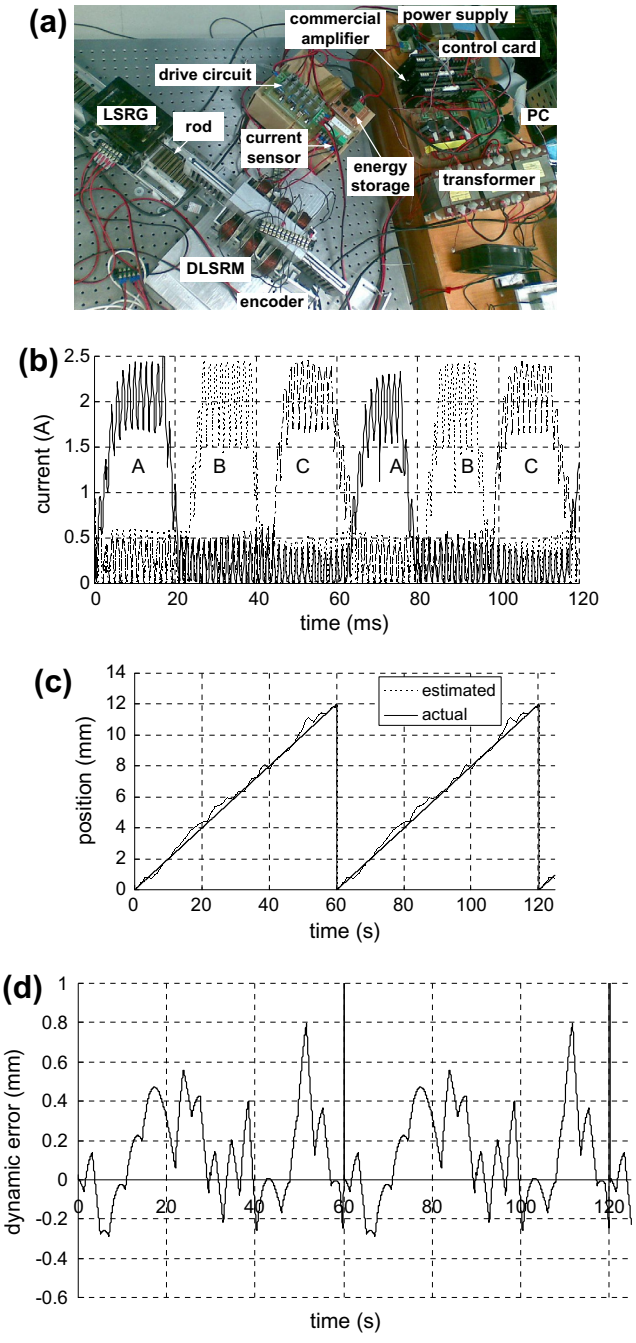

Fig. 11. (a) Experimental setup (b) three-phase current (c) position estimation profile and (d) dynamic error at 0.2 m/s.

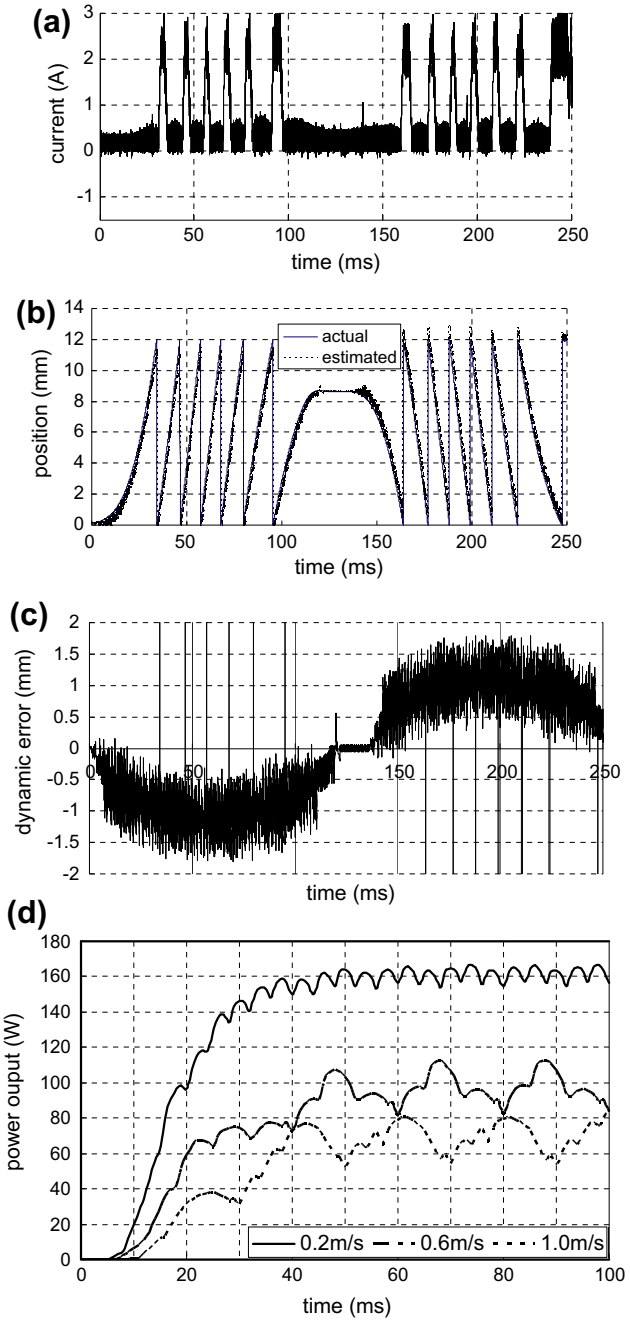

Fig. 12. Experimental results of (a) current waveforms under sinusoidal speed (b) estimated position profiles (c) dynamic position error and (d) power output at different speeds.

from the waveforms that output power increases with the propulsion speed inversely. According to Eq. (12), average efficiency values of the LSRG-based system at 0.2, 0.6 and 1 m/s are evaluated as 34.7%, 39.3% and 45.8%, respectively.

Conclusion and discussion

A direct-drive, LSRG-based power generation control system for wave energy exploitation integrated with sensorless technique is discussed in this paper. The generator has the characteristics of a stable and robust machine structure. Combined with the position estimation method, the overall cost of the generation system can be further reduced and it is suitable for operation under hostile environment. The performance of the LSRG-based generation system has been investigated. Both simulation and experimental results prove the effectiveness of the position estimation scheme and closed loop current regulation. It is expected that the LSRG-based sensorless generation system find its applications for wave energy utilization.

For typical LSPMGs, the introduction of PMs inevitably affects the performance of the machines. Moreover, the involvement of physical sensors or transducers from linear generators makes the power generation control system vulnerable to the variations of wave extraction environments. Therefore, the LSRG based wave utilization system is more reliable to direct-drive systems with physical sensors.

From the above, the detection of the relative positions between phase movers to the stator can effectively help correct current excitation or power generation. If the moving platform reaches the end limit of either side, the detection scheme is no longer available without mechanical assistance such as springs or dampers, to prevent the moving platform from collision to the two sides. Therefore, it is suggested that the absolute position detection technique and corresponding control such as self braking be employed for the LSRG based power generation control system in the forthcoming study.

Acknowledgments

This work was supported by the National Natural Science Foundation of China under Grant 51007059 and Grant 51275312 and by the Guangdong Natural Science Foundation under Grant S2011010001208. The authors would also like to thank Shenzhen government under the code of JCYJ20130329144017199 for support.

References

[1] Falcão António Fde O. Wave energy utilization: a review of the technologies. J Renew Sust Energy Rev 2010;14:899–918.
[2] Scruggs J, Jacob P. Harvesting ocean wave energy. Science 2009;323:1176–8.
[3] Henderson R. Design, simulation, and testing of a novel hydraulic power take-off system for the Pelamis wave energy converter. J Renew Energy 2006;31:271–83.
[4] Kofoed J, Frigaard P, Madsen E, Sørensen H. Prototype testing of the wave energy converter wave dragon. J Renew Energy 2006;31:181–9.
[5] Valério D, Beirão P, Sá da Costa J. Optimisation of wave energy extraction with the Archimedes Wave Swing. J Ocean Eng 2007;34:2330–44.
[6] Langhamer O, Haikonen K, Sundberg Jan. Wave power-sustainable energy or environmentally costly? a review with special emphasis on linear wave energy converters. J Renew Sust Energy Rev 2010;14:1329–35.
[7] Lee S, Kim S, Zhu Y, Cho Y. Optimal Structure design for minimizing detent force of PMLSM for a ropeless Eeevator. IEEE Trans Magn 2014;50:4001104.
[8] Jian C, Ma W, Fan Y, Yang H. New methods for arc permanent magnet linear synchronous motor to decrease torque ripple. IEEE Trans Magn 2012;48:2659–63.
[9] Ivanova A, Ågren O, Bernhoff H, Leijon MS. Simulation of wave-energy converter with octagonal linear generator. IEEE J Oceanic Eng 2005;30:619–29.
[10] Choi C, Lee W, Kwon S, Hong J. Experimental estimation of inductance for interior permanent magnet synchronous machine considering temperature distribution. IEEE Trans Magn 2013;49:2990–6.
[11] Dorf R, Bishop RH. Modern control systems. 10th ed. New York: Prentice Hall; 2004.
[12] Krishnan R. Switched reluctance motor drives: modeling, simulation, analysis, design, and applications. 1st ed. U.S.: CRC Press; 2001.
[13] Guo H, Takahashi M, Watanabe T, Ichinokura O. A new sensorless drive method of switched reluctance motors based on motor's magnetic characteristics. IEEE Trans Magn 2001;37:2831–3.
[14] Zhao S, Cheung N, Gan W, Yang J. Position estimation and error analysis in linear switched reluctance motors. IEEE Trans Ind Instrum Meas 2009;58:2815–23.
[15] Zhao S. Robust and sensorless control of linear switched reluctance motors, PhD thesis, The Hong Kong Polytechnic University; 2008.
[16] Carballo R, Iglesias G. A methodology to determine the power performance of wave energy converters at a particular coastal location. J Energy Convers Manage 2012;61:8–18.
[17] Pan J, Zou Y, Cao G. Investigation of a low-power, double-sided switched reluctance generator for wave energy conversion. IET Renew Power Gener 2013;7:98–109.
[18] Miller TJ. Electronic control of switched reluctance machines. 1st ed. Newnes Power Engineering Series, U.S.; 2001.